RESEARCH ARTICLE
SPACE PHYSICS: MAGNETOSPHERIC PHYSICS

Earth and Planetary Physics
4: 131–137, 2020
doi: 10.26464/epp2020019

Evolutions of equatorial ring current ions during a magnetic storm

Zheng Huang, ZhiGang Yuan*, and XiongDong Yu

School of Electronic Information, Wuhan University, Wuhan 420072, China

Key Points:

- Ring current ions with low magnetic moment values can penetrate deeper into the magnetosphere than those with high magnetic moment values during a storm main phase
- Both satellite observations and theoretical calculation show the efficiency of the radial transport for RC ions into the deep inner magnetosphere caused by drift-bounce resonance interactions, meets $\eta(O^+) > \eta(He^+) > \eta(H^+)$
- In the recovery phase of a moderate storm, the observed decay rates for different RC ions meet the relationship: $R(O^+) > R(He^+) > R(H^+)$

Citation: Huang, Z., Yuan, Z. G., and Yu, X. D. (2020). Evolutions of equatorial ring current ions during a magnetic storm. *Earth Planet. Phys.*, *4*(2), 131–137. http://doi.org/10.26464/epp2020019

Abstract: In this paper, we present evolutions of the phase space density (PSD) spectra of ring current (RC) ions based on observations made by Van Allen Probe B during a geomagnetic storm on 23–24 August 2016. By analyzing PSD spectra ratios from the initial phase to the main phase of the storm, we find that during the main phase, RC ions with low magnetic moment μ values can penetrate deeper into the magnetosphere than can those with high μ values, and that the μ range of PSD enhancement meets the relationship: $S(O^+) > S(He^+) > S(H^+)$. Based on simultaneously observed ULF waves, theoretical calculation suggests that the radial transport of RC ions into the deep inner magnetosphere is caused by drift-bounce resonance interactions, and the efficiency of these resonance interactions satisfies the relationship: $\eta(O^+) > \eta(He^+) > \eta(H^+)$, leading to the differences in μ range of PSD enhancement for different RC ions. In the recovery phase, the observed decay rates for different RC ions meet the relationship: $R(O^+) > R(He^+) > R(H^+)$, in accordance with previous theoretical calculations, i.e., the charge exchange lifetime of O^+ is shorter than those of H^+ and He^+.

Keywords: ULF waves; ring current; wave-particle interactions; radial transport; geomagnetic storm; decay rates

1. Introduction

Ring current (RC) consists of plasma ions with energy from 1 keV to several hundred keV that are trapped by the Earth's magnetic field (Daglis et al., 1999). Its main positive ions are of hydrogen, helium, and oxygen. In quiet times, the ring current is composed primarily of hydrogen ions; during storm times, the proportion of oxygen ions becomes considerable and in very intense magnetic storms may become the dominant ion species in the ring current (e.g., Gloeckler et al., 1985; Hamilton et al., 1988; Greenspan and Hamilton, 2002; Keika et al., 2013; Yue C et al., 2018, 2019). In general, the near-Earth plasma sheet contains mixed particles from the ionosphere (H^+, O^+, He^+) and solar wind (H^+, He^+, He^{++}), which is generally considered to be a direct source of ring current ions (Daglis, 2006).

The ULF (Ultra-Low-Frequency) wave range, also known as the range of geomagnetic pulsation, is defined to be from 1 Hz to 1 mHz. Many studies have been made of ULF wave generation and effects (e.g. Liu ZY et al., 2019; Zong Q-G et al., 2009, 2012). The sources of ULF waves in the Earth's magnetosphere are generally thought to be external solar wind disturbances and internal plasma instabilities (Liu W et al., 2013). Solar wind pressure pulses are considered to be an important external source of ULF wave excitation (Shi QQ et al., 2013, 2014). Positive solar wind pressure pulses, i.e., sudden increases in solar wind pressure, can compress the magnetosphere. The interaction between the geomagnetic field and positive solar wind pressure pulses has been shown to excite ULF waves in the inner magnetosphere (Zhang XY et al., 2010; Liu W et al., 2013). Other important sources of ULF waves include Kelvin–Helmholtz instability, interplanetary shock, foreshock transients, and so on (Claudepierre et al., 2008; Zong Q-G et al., 2009, 2012; Hartinger et al., 2013).

ULF waves with periods close to the drift and bounce motion cycles of energetic particles can affect the dynamics of ring current ions by drift or drift-bounce resonance (Dai L et al., 2013; Zong Q-G et al., 2017). This process involves adiabatic acceleration of inner magnetosphere ions and significant enhancements of their radial diffusion (Elkington et al., 2003; Loto'aniu et al., 2006). Oxygen ions with energies from 10 keV to 500 keV are more likely to resonate with ULF waves than hydrogen ions (Zong Q-G et al., 2012), which may lead to the radial diffusion of oxygen ions. Mitani et al., (2018) have proposed that drift-bounce resonance can facilitate the penetration of O^+ ions from the plasma sheet into the deep inner magnetosphere. Yang B et al. (2011) reported

Correspondence to: Z. G. Yuan, y_zgang@vip.163.com
Received 19 NOV 2019; Accepted 10 JAN 2020.
Accepted article online 24 FEB 2020.

the acceleration of 10–25 keV O^+ and deceleration of 4–8 keV O^+ through drift-bounce resonance. However, there have been few comprehensive studies of the interaction of ULF waves with different kinds of energetic ions (H^+, He^+, O^+) in the ring current region; the transport mechanism of ring current ions entering the deep inner magnetosphere is not clear. In addition, previous studies have observed a more rapid loss of O^+ ions than of H^+ ions in the recovery phase of super magnetic storms (Hamilton et al., 1988; Daglis 1997). During the recovery phase of the moderate magnetic storm studied in this paper, we observe the same phenomenon.

In this paper, we will study the transport process by analyzing the phase space density (PSD) of RC ions in the radial range L ~ 3–5 and magnetic moment range μ ~ 0.1–2.0 keV/nT during storm times, so as to reveal the control mechanism of ring current ion evolution during the different phases of geomagnetic storms.

2. Observation

The RBSP (Radiation Belt Storm Probes) mission contains two functionally equivalent spacecrafts: RBSP-A and RBSP-B. Their near-equatorial orbits have a period of ~9 hours, an apogee altitude of ~5.8R_E, a perigee altitude of ~600 km, and an inclination of ~10°. Each satellite has five nearly identical instrument suites that measure particles over a wide range of energy and species, as well as electromagnetic fields over a wide range of frequencies (Mauk et al., 2013). In this study, we used ion flux data from the Radiation Belt Storm Probes Ion Composition Experiment (RBSPICE) (Mitchell et al., 2013) and magnetic field data from the Electric and Magnetic Field Instrument Suite and Integrated Science (EMFISIS) project (Kletzing et al., 2013) on board the RBSP-B satellite. The RBSPICE is a plasma spectrometer that detects the energy range of ~50–600 keV in 14 energy channels for protons, ~60–870 keV in 11 energy channels for Helium ions, and 140–870 keV in 8 energy channels for oxygen ions. The EMFISIS suite includes magnetic field and wave detectors with different time resolutions. We select the magnetic field data with 1 second time resolution. Solar wind information and geomagnetic index are obtained from OMNI data with 1 min time resolution.

In this study, we conducted an investigation of the magnetic storm on 23–24 August 2016, with observations from RBSP-B. Figure 1 displays an overview of the event. The first four panels (a–d) show the *AE* (Auroral Electrojet) index, the SYM-*H* (Symmetric Horizontal component of geomagnetic disturbance) index, IMF B_z in GSM coordinate (z component of interplanetary magnetic field) and Pressure (dynamic pressure of solar wind). As shown in panel (b), the magnetic storm began at approximately 11:35 UT on 23 August. The red vertical solid lines on the panels (a)–(d) divide the magnetic storm into three stages, i.e., the initial phase, the main phase, and the recovery phase. The three intervals denoted by pink vertical dashed lines on the flux panel correspond to the satellite orbits of L ~ 3–5 in the three stages of the geomagnetic storm. Between the two vertical pink solid lines, the SYM-*H*

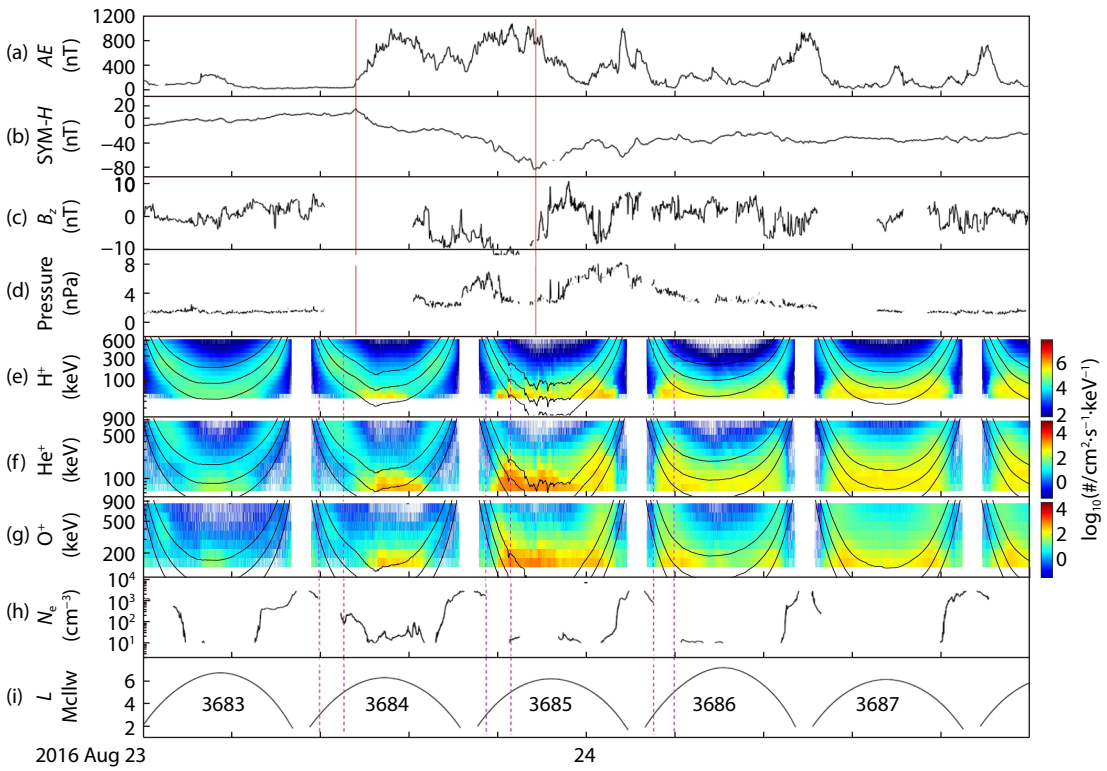

Figure 1. Overview of magnetic storm events that occurred from 23–24 August 2016 : (a) *AE* index, (b) SYM-*H* index, (c) IMF B_z, (d) Solar wind dynamic pressure from OMNI data set; (e, f, g) Omnidirectional flux of hydrogen, helium, and oxygen ions detected by RBSPICE; the three black solid lines on flux panels represent μ = 0.3 keV/nT, 0.6 keV/nT, 1 keV/nT from bottom to top; (h, i) Electron number density and L-McIlwain value. The red solid interval on the *Dst* index panel indicates the main phase, the pink vertical dotted lines denote the interval of L ~ 3–5 on Orbit 3864 in the initial phase, Orbit 3865 in the main phase, and Orbit 3866 in the recovery phase, respectively.

index dropped from 16 nT to –23 nT, then slowly reverted to –17 nT, thereafter dropping to the minimum point, –83 nT, at ~21:18 UT, indicating a moderate magnetic storm (Kamide et al., 1998). During the main phase, the *AE* index displays strong enhancements, implying strong injections of plasma sheet ions into the inner magnetosphere. IMF B_z is southward (i.e., negative) in the main phase. The solar wind dynamic pressure gradually increases to ~7 nPa, leading to the excitation of ULF waves, as shown below. These solar wind conditions meet the characteristics of a corotating interaction region-driven (CIR-driven) storm (e.g., Borovsky and Denton, 2006; Kamide et al., 1998). The next three flux panels show the omnidirectional flux of hydrogen ions, helium ions, and oxygen ions, respectively. The three black solid lines on each flux panel mark the magnetic moments of 0.3, 0.6, and 1.2 keV/nT, respectively. The actual calculation is for 0.1, 0.2, …, 2.0 keV/nT ions with intervals of 0.1 keV/nT. Panels (h) and (i) show the electron number density N_e and satellite's position given the McIlwain-*L* value. Here we focus on Orbits 3684 in *L* ~ 3–5 (the initial phase) and 3685 in *L* ~ 3–5 (the main phase). For convenience, the pink dotted line interval is replaced with the orbit number. As shown in Figure 1e, during the main phase (Orbit 3685 in *L* ~ 3–5), only low-energy (<60 keV) hydrogen ion flux was enhanced in the inner magnetosphere. During the recovery phase (Orbit 3686 in *L* ~ 3–5), the flux of high-energy (>100 keV) hydrogen ions also was enhanced. In contrast, as shown in Figures 1(f–g), the fluxes of both low-energy (<150 keV) and high-energy (>150 keV) heavy ions (He^+, O^+) were enhanced in the inner magnetosphere during the main phase (Orbit 3685 in *L* ~ 3–5). The difference in behavior between heavy ions (He^+, O^+) and hydrogen ions (H^+) in the main phase indicates that high-energy heavy ions can be effectively injected into the inner magnetosphere.

To further study the adiabatic diffusion process of RC ions during magnetic storms, we calculated the phase space density (PSD) of RC ions in the radial range *L* ~ 3–5 and magnetic moment range μ ~ 0.1–2.0 keV/nT during the magnetic storm (from Orbit 3684 to 3686), shown in Figure 2(a–i). The radial ranges *L* ~ 3–5 of Orbits 3684, 3685, 3686 correspond to the initial phase, the main phase, and the recovery phase, respectively. Note that the PSD spectra versus *L* and μ is converted by flux data as well as magnetic field data. The PSD spectra in *L*–μ space can allow us to trace the evolution of RC ions during the magnetic storms. We select particles with a pitch angle of ~90° (the actually measured pitch angle range of the particles is 85°–95°). Next, PSD, or $f_\perp$, is calculated for each energy channel by

$$f_\perp = A \cdot \frac{j_\perp}{E}, \tag{1}$$

where $f_\perp$ is the perpendicular PSD, $j_\perp$ is the ions differential flux with 90° pitch angle, *E* is the midpoint energy of the ion energy channel, and the *A* is the conversion factor that is used to convert $j_\perp$(units of $cm^{-2}{\cdot}s^{-1}{\cdot}sr^{-1}{\cdot}keV^{-1}$) into $f_\perp$(units of s^3/km^6) for energy *E* (units of keV). The values of *A* for hydrogen, helium, and oxygen ions are 5.449×10^{-31}, 8.7185×10^{-30} and 1.3950×10^{-28}, respectively (Lyons and Williams., 1984). We first calculate the PSD of all energy channels at *L* ~ 3–5, and then filter out the ion PSD corresponding to the specific magnetic moment (μ = 0.1, 0.2, …, 2.0 keV/nT). As a result, the PSD spectra in *L*–μ space can be obtained.

Figure 2 shows phase space density spectra of RC ions (μ ~ 0.1–2.0 keV/nT) during the magnetic storm, corresponding to Orbits 3684, 3685, and 3686 in *L* ~ 3–5, respectively. Figures 3(a–c), (d–f) and (g–i) are for hydrogen ions, helium ions, and oxygen ions. The PSD spectra reflect the evolution of RC ions with different μ values: one group with lower PSD values (<~10^3 s^3/km^6 for H^+, <~10^2 s^3/km^6 for He^+, O^+) shows the pre-existing ring current ions, and another group with higher PSD values (>~10^3 s^3/km^6 for H^+, >~10^2 s^3/km^6 for He^+, O^+) shows the ions injected from the plasma sheet. For ions with a specific magnetic moment value, when phase space density starts to increase significantly, we define the corresponding *L* value as the inner edge position. In order to better identify the inner edge position of RC ions with different μ values during storm times, we adopt the ion PSD ratio of Orbit 3685 to Orbit 3684, which is shown in Figures 2(j–l). During the main phase of the magnetic storm, the inner edge of RC ions with lower μ value (<0.3 keV/nT for H^+, <0.6 keV/nT for He^+, <1.0 keV/nT for O^+) can be observed obviously moving into *L* < 4.4. As shown in Figures 2(j–l), from the initial phase to the main phase (from Orbit 3684 to Orbit 3685), the μ ranges (*S*) of PSD enhancement for RC ions are satisfied: $S(O^+) > S(He^+) > S(H^+)$. As ions penetrate deeper into the inner magnetosphere, the magnitude of PSD enhancement decreases gradually. As shown in Figures 2(m–o), from the main phase to the recovery phase (from Orbit 3685 to Orbit 3686), the flux of hydrogen ions with lower μ values seemed to penetrate deeper while the heavy ion flux decreased (i.e., indicating decay of RC heavy ions).

3. Discussion

The interaction between ULF waves and inner-magnetosphere RC ions is considered an effective mechanism for the radial diffusion of energetic RC ions (Elkington et al. 2003; Loto'aniu et al. 2006; Zong Q-G et al., 2012; Mitani et al., 2018). In order to check whether RC ions are transported into the inner magnetosphere by interacting with the ULF waves, we examined the magnetic fluctuations in these orbits and found that there were few obvious signs of ULF fluctuations during Orbit 3684 in *L* ~ 3–5 (initial phase), but very strong ULF fluctuations were observed during Orbit 3685 in *L* ~ 3–5 (main phase), indicating that enhancements of ULF fluctuations occurred in the main phase. At the same time, as shown in Figures 2(j–l), the phase space density ratios of Orbit 3685 and Orbit 3684 also indicate that RC ion PSDs were enhanced during the main phase. The comparison of the two enhanced activities implies that the enhancement of RC ion PSDs may be related to the enhancement of ULF fluctuations during magnetic storms.

Figure 3 displays the power spectra density of magnetic field fluctuations in the first, second, and third pink intervals shown in Figure 1, corresponding to the initial phase (Orbit 3684 in *L* ~ 3–5), the main phase (Orbit 3685 in *L* ~ 3–5), and the recovery phase (Orbit 3686 in *L* ~ 3–5), respectively. From top to bottom, three panels represent the poloidal, toroidal, and compressional component of magnetic field fluctuations, abbreviated by ΔB_{pol}, ΔB_{tor}, ΔB_{com}. In particular, the poloidal component of magnetic fluctuations can induce toroidal electric oscillation, thus facilitating wave-particle interaction (Mitani et al., 2018). Comparing those on Orbit 3684 and Orbit 3685, the poloidal component of magnetic

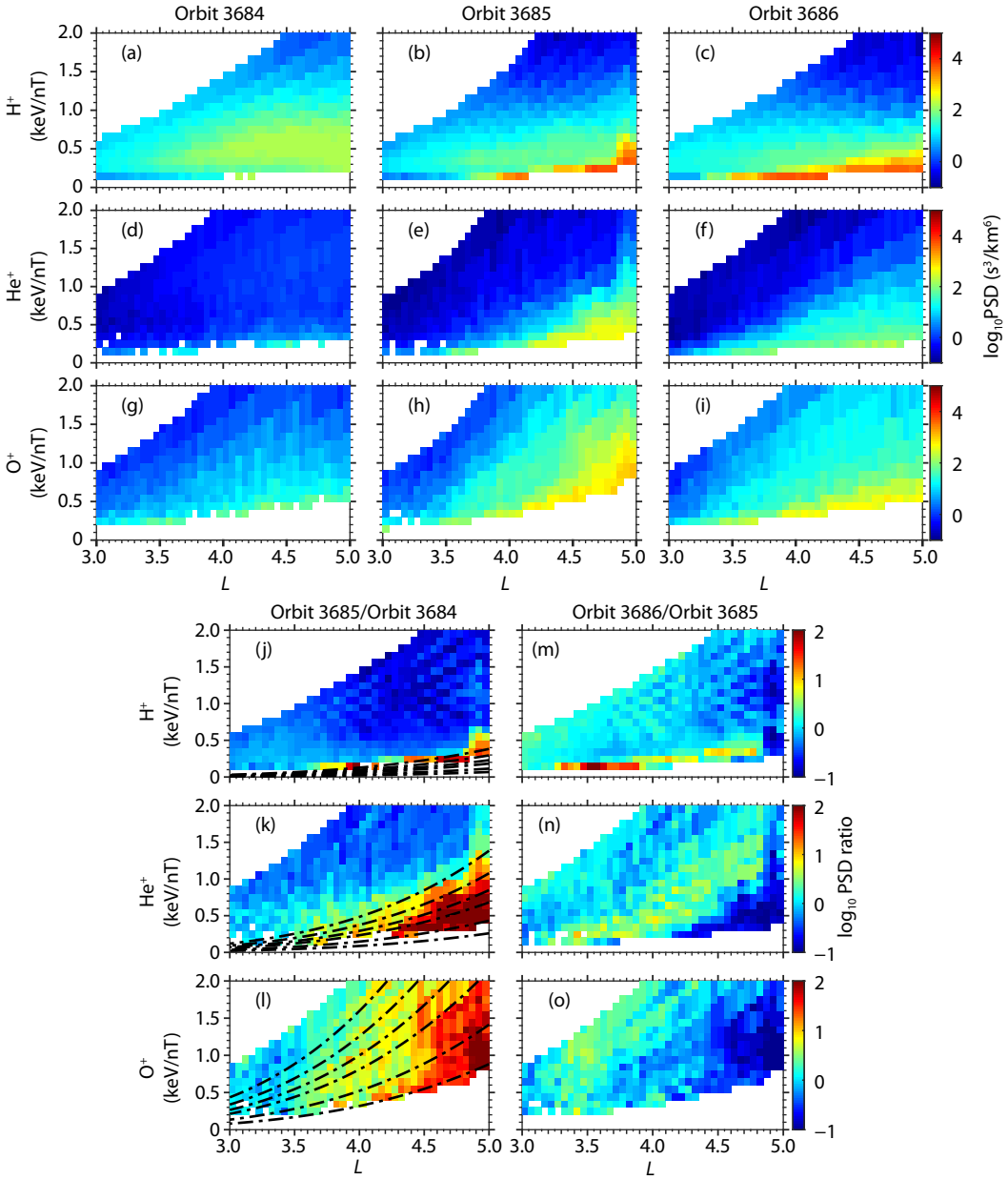

Figure 2. The PSD spectra of RC ions in L–μ space (μ ~ 0–2 keV/nT, L ~ 3–5) on Orbits 3684, 3685 and 3686, respectively. (a–c) PSD spectra for hydrogen ions; (d–f) PSD spectra for Helium ions; (g–i) PSD spectra for Oxygen ions; (j, k, l) PSD ratio spectra of Orbit 3685 and Orbit 3684 for RC ions. (m, n, o) PSD ratio spectra of Orbit 3686 and Orbit 3685 for RC ions. The black dotted lines plotted on panels (j, k, l) with various frequencies, satisfy drift-bounce resonance conditions $N = 1$, $m = 5$. ULF waves frequencies for black lines are 20, 26, 33, 37, 42, and 48 mHz from bottom to top, respectively.

field fluctuation shows significant enhancement, while the compressional component of magnetic field fluctuation is the most significant among the three components. On Orbit 3685 in $L > 4.1$, the magnetic field fluctuations with frequencies from several mHz to several tens of mHz are enhanced, while in L ~ 4.1–3.5, the magnetic field fluctuations are concentrated mainly in the 1–50 mHz range.

Figure 4 shows the resonance region theoretically calculated in the resonance condition when RC ions interact with ULF waves by drift-bounce resonance. The left, middle, and right two columns are for H^+, He^+, O^+, respectively. The drift-bounce resonance condition of energetic particles is expressed as (Southwood et al., 1969)

$$\omega - m\omega_d = N\omega_b, \tag{2}$$

where ω is the wave frequency, m is the azimuthal mode number, ω_d is the ion drift frequency, N is an integer which depends on the wave harmonics, and ω_b is the ion bounce frequency, respectively. In a dipole magnetic field, the frequencies ω_b and ω_d about ion bounce and drift motion can be numerically approximated by (Baumjohann and Treumann, 1997)

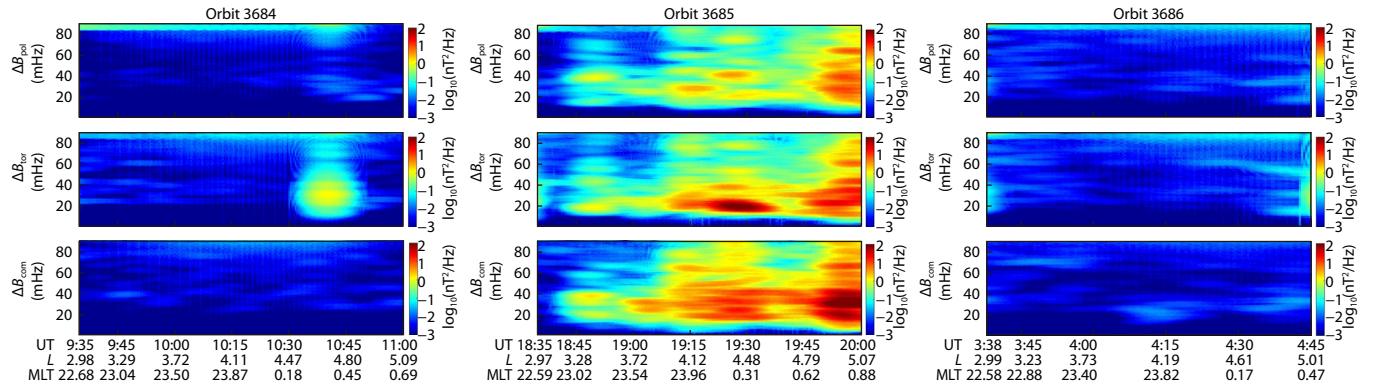

Figure 3. Observations by RBSP-B EMFISIS in L ~ 3–5 of Orbits 3864, 3685, and 3686: power spectra of ΔB_{pol}, ΔB_{tor}, ΔB_{com} (poloidal, toroidal, compressional) of the magnetic fluctuations.

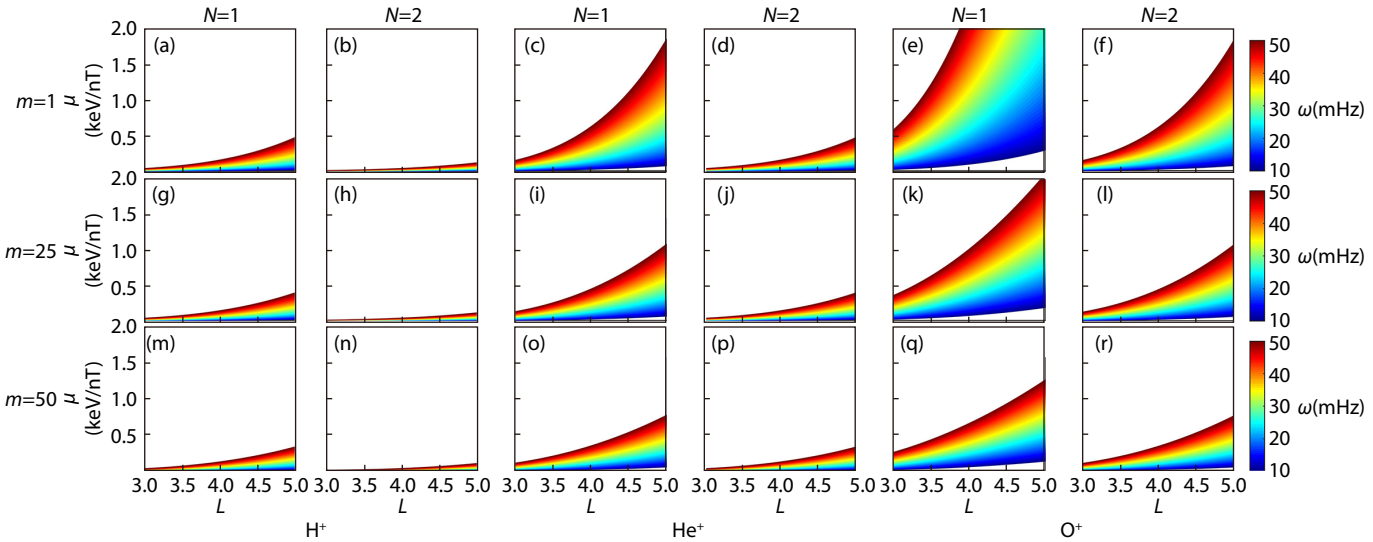

Figure 4. Under the condition of dipole magnetic field, the resonance region in L–μ space when the ring current ions satisfy the drift-bounce resonance interaction with the ULF wave according to the resonance condition equation. The two columns on the left correspond to H^+; the middle two columns correspond to He^+; the two columns on the right correspond to O^+; and for each ion species, the first and second columns correspond to the cases of N = 1, 2, the first, second, and third rows corresponding to the cases of m=1, 25, and 50, respectively.

$$\omega_b = \frac{(W/m_i)^{1/2}}{LR_E}\left(3.7 - 1.6\sin\alpha_{eq}\right)^{-1}, \quad (3)$$

$$\omega_d = \frac{3LW}{\pi q B_E R_E^2}\left(0.35 + 0.15\sin\alpha_{eq}\right), \quad (4)$$

where W is the ion energy, m_i is the ion mass, L is the dipole field L-shell parameter, R_E is the radius of the Earth, α_{eq} is the pitch angle at the geomagnetic equator, B_E is the equatorial magnetic field on the Earth's surface, and q is the ion charge. Both drift frequency and bounce frequency depend on particle energy W, L, and equatorial pitch angle α_{eq}. Given the assumption $\alpha_{eq} = 90°$, we have $W \approx W_\perp$, so that ω_b, ω_d can be converted into a function of μ and L. After inserting Equations (3) and (4) into Equation (2), we obtain a function about μ and L, once parameters ω, m, and N are specified. So far we have theoretically established a link between RC ions and ULF waves to perform the drift-bounce resonance. Figure 4 reveals how the wave frequency, ion species, azimuthal mode number, and resonance harmonics affect the efficiency of drift-bounce resonance interactions.

As shown in Figure 4, for a specific ion, when N (or m) is a definite value, the resonance range in μ–L space decreases as m (or N) increases; N has a stonger influence on the resonance region than m. For different kinds of ions, under the same m and N the resonance range (or interaction efficiency, η) in μ–L space meets: $\eta(O^+) > \eta(He^+) > \eta(H^+)$. Therefore it can be explained why the low-energy (<~60 keV) hydrogen ion flux in Figure 1e was enhanced, while the high-energy (>~100 keV) hydrogen ion flux was not significantly enhanced in the main phase of the geomagnetic storm; that is, only hydrogen ions of lower μ values interact with ULF waves, resulting in PSD enhancement of hydrogen ions with lower μ values, which is shown in Figure 2j; in comparison, Figures 1(f, g) show that fluxes of both low and high-energy heavy ions (He^+, O^+) were significantly enhanced, which is consistent with a larger resonance μ range when the heavy ions interact with ULF wave, shown in Figures 2(k, l). Combined with the PSD ratio spectra of Figures 2(j–l), it can be found that the resonance region calculated by N = 1, m < 25 is most consistent with the observed PSD enhancement. The black solid lines in the PSD ratio spectra of

Figures 2(j–l) represents a series of (L, μ) values meeting the drift-bounce condition with N = 1, m = 5, and ULF waves with 20, 26, 33, 37, 42, and 48 mHz. At the same time, the RBSP-B satellite also observed enhancements of magnetic field fluctuations with frequencies of 10–50 mHz for L < 4.4 during the main phase, further confirming that the radial injection of RC ions into the deep inner magnetosphere is caused by drift-bounce resonance.

Drift resonance (N = 0) is not considered here since the velocity of $\boldsymbol{E}\times\boldsymbol{B}$ drift does not depend on the ion mass, so the penetration depth through $\boldsymbol{E}\times\boldsymbol{B}$ drift alone should be the same for different kinds of RC ions with same μ; i.e., the μ range of PSD enhancement for each kind of RC ion should be the same. However, although the three main ions of the ring current have been observed to penetrate into the deep inner magnetosphere, the μ range of PSD enhancement is more expanded as the ion mass becomes heavier. Thus, drift-bounce resonance is considered to explain the μ range discrepancies for different RC ions.

The fiux increase of O^+ ions in the magnetosphere affects not only the enhancement of the ring current in the main phase, but also affects the decay rate of the ring current in the recovery phase, because for ring current energies above 40 keV the charge exchange lifetime of O^+ ions is much shorter than the lifetime of H^+ ions (Smith and Bewtra, 1978; Kozyra et al., 1997). In this study, from the main phase to the recovery phase (from Orbit 3685 to Orbit 3686), the decay rates for different components of RC ions meet: $R(O^+) > R(He^+) > R(H^+)$, which is shown in Figures 2(m–o). This result illustrates that the decay rate for different RC ions in a moderate magnetic storm also satisfies the above relationship.

4. Summary

Based on observations made on satellite RBSP-B during the magnetic storm on 23–24 August 2016, the evolution of equatorial ring current ions in the different phases of the magnetic storm is studied. The main results are as follows:

(1) When a magnetic storm occurs, the μ ranges of PSD enhancement for different ring current ions meets: $S(O^+) > S(He^+) > S(H^+)$. For all kinds of RC ions, it is almost satisfied that ions of lower μ values can penetrate further into the inner-magnetosphere (minimum L ~ 3.6) than can those of higher μ values. As ions penetrate deeper into the inner magnetosphere, the magnitude of PSD enhancement decreases gradually.

(2) There were few obvious signs of ULF fluctuations in the initial phase, while very strong ULF fluctuations with frequencies of 1–50 mHz were simultaneously observed in the radial ranges of PSD enhancement during the main phase.

(3) Using the resonance equation, the resonance region of the interaction between observed ULF wave and RC ions in the L–μ space (μ ~ 0.1–2.0 keV/nT, L ~ 3–5) is calculated under the condition of dipole magnetic field. The calculated resonance region implies that the resonance efficiency of RC ions meets: $\eta(O^+) > \eta(He^+) > \eta(H^+)$, demonstrating that the μ range difference of PSD enhancement among RC ions is caused by the difference in resonance efficiency between RC ions and ULF waves.

(4) In the recovery phase, the decay rates for different components of RC ions meet: $R(O^+) > R(He^+) > R(H^+)$, i.e., the charge exchange lifetime of O^+ is shorter than those of He^+ and H^+.

Ring current is an important part of the magnetosphere. By studying evolutions of the radial distribution of the main ions in different stages of a magnetic storm, we find that ring current ions can penetrate the deep inner magnetosphere through drift-bounce resonance, and that differences in resonance efficiency are observed among the three kinds of main ions. We conclude that the 1–50 mHz ULF waves can play an important role in the supply of lower μ RC ions injected into the inner magnetosphere during storm times. At the same time, we have also confirmed the difference in decay rates caused by differences in charge exchange lifetimes among RC ions.

Acknowledgments

We acknowledge the Van Allen Probes data from the EMFISIS and HOPE instruments, obtained from https://cdaweb.gsfc.nasa.gov/pub/data/rbsp/rbspb/l3/. The Solar dynamic pressure, *AE* index and *Dst* index data were provided by SPDF OMNI web at http://omniweb.gsfc.nasa.gov/. This work is supported by the National Natural Science Foundation of China (41925018, 41874194).

References

Baumjohann, W., and Treumann, R. A. (1997). Basic Space Plasma Physics. London: Imperial College Press.

Borovsky, J. E., and Denton, M. H. (2006). Differences between CME-driven storms and CIR-driven storms. *J. Geophys. Res. Space Phys.*, *111*(A7), A07S08. https://doi.org/10.1029/2005JA011447

Claudepierre, S. G., Elkington, S. R., and Wiltberger, M. (2008). Solar wind driving of magnetospheric ULF waves: Pulsations driven by velocity shear at the magnetopause. *J. Geophys. Res. Space Phys.*, *113*(A5), A05218. https://doi.org/10.1029/2007JA012890

Daglis, I. A. (1997). The role of magnetosphere-ionosphere coupling in magnetic storm dynamics. In B. T. Tsurutani, et al. (Eds.), Magnetic Storms (Vol. 98, pp. 107–116). Washington, DC: American Geophysical Union. https://doi.org/10.1029/GM098p0107

Daglis, I. A., Thorne, R. M., Baumjohann, W., and Orsini, S. (1999). The terrestrial ring current: Origin, formation, and decay. *Rev. Geophys.*, *37*(4), 407–438. https://doi.org/10.1029/1999RG900009

Daglis, I. A. (2006). Ring current dynamics. *Space Sci. Rev.*, *124*(1-4), 183–202. https://doi.org/10.1007/s11214-006-9104-z

Dai, L., Takahashi, K., Wygant, J. R., Chen, L., Bonnell, J., Cattell, C. A., Thaller, S., Kletzing, C., Smith, C. W., … Spence, H. E. (2013). Excitation of poloidal standing Alfvén waves through drift resonance wave-particle interaction. *Geophys. Res. Lett.*, *40*(16), 4127–4132. https://doi.org/10.1002/grl.50800

Elkington, S. R., Hudson, M. K., and Chan, A. A. (2003). Resonant acceleration and diffusion of outer zone electrons in an asymmetric geomagnetic field. *J. Geophys. Res. Space Phys.*, *108*(A3), 1116. https://doi.org/10.1029/2001JA009202

Gloeckler, G., Wilken, B., Stüdemann, W., Ipavich, F. M., Hovestadt, D., Hamilton, D. C., and Kremser, G. (1985). First composition measurement of the bulk of the storm-time ring current (1 to 300 keV/e) with AMPTE-CCE. *Geophys. Res. Lett.*, *12*(5), 325–328. https://doi.org/10.1029/GL012i005p00325

Greenspan, M. E., and Hamilton, D. C. (2002). Relative contributions of H^+ and O^+ to the ring current energy near magnetic storm maximum. *J. Geophys. Res. Space Phys.*, *107*(A4), SMP 3-1–SMP 3-9. https://doi.org/10.1029/2001JA000155

Hamilton, D. C., Gloeckler, G., Ipavich, F. M., Stüdemann, W., Wilken, B., and Kremser, G. (1988). Ring current development during the great geomagnetic storm of February 1986. *J. Geophys. Res. Space Phys.*, *93*(A12),

14343–14355. https://doi.org/10.1029/JA093iA12p14343

Hartinger, M. D., Turner, D. L., Plaschke, F., Angelopoulos, V., and Singer, H. (2013). The role of transient ion foreshock phenomena in driving Pc5 ULF wave activity. *J. Geophys. Res. Space Phys.*, *118*(1), 299–312. https://doi.org/10.1029/2012JA018349

Kamide, Y., Baumjohann, W., Daglis, I. A., Gonzalez, W. D., Grande, M., Joselyn, J. A., McPherron, R. L., Phillips, J. L., Reeves, E. G. D., … Vasyliunas, V. M. (1998). Current understanding of magnetic storms: Storm-substorm relationships. *J. Geophys. Res. Space Phys.*, *103*(A8), 17705–17728. https://doi.org/10.1029/98JA01426

Keika, K., Kistler, L. M., and Brandt, P. C. (2013). Energization of O^+ ions in the Earth's inner magnetosphere and the effects on ring current buildup: A review of previous observations and possible mechanisms. *J. Geophys. Res. Space Phys.*, *118*(7), 4441–4464. https://doi.org/10.1002/jgra.50371

Kletzing, C. A., Kurth, W. S., Acuna, M., MacDowall, R. J., Torbert, R. B., Averkamp, T., Bodet, D., Bounds, S. R., Chutter, M., … Tyler, J. (2013). The Electric and Magnetic Field Instrument Suite and Integrated Science (EMFISIS) on RBSP. *Space Sci. Rev.*, *179*(1-4), 127–181. https://doi.org/10.1007/s11214-013-9993-6

Kozyra, J. U., Jordanova, V. K., Home, R. B., and Thorne, R. M. (1997). Modeling of the contribution of electromagnetic ion cyclotron (EMIC) waves to stormtime ring current erosion. In B. T. Tsurutani, et al. (Eds.), Magnetic Storms (pp. 187-202). Washington, DC: American Geophysical Union. https://doi.org/10.1029/GM098p0187

Liu, W., Cao, J. B., Li, X., Sarris, T. E., Zong, Q. Z., Hartinger, M., Takahashi, K., Zhang, H., Shi, Q. Q., and Angelopoulos, V. (2013). Poloidal ULF wave observed in the plasmasphere boundary layer. *J. Geophys. Res. Space Phys.*, *118*(7), 4298–4307. https://doi.org/10.1002/jgra.50427

Liu, Z. Y., Zong, Q.-G., Zhou, X. Z., Hao, Y. X., Yau, A. W., Zhang, H., Chen, X. R., Fu, S. Y., Pollock, C. J., … Lindqvist, P. A. (2019). ULF waves modulating and acting as mass spectrometer for dayside ionospheric outflow ions. *Geophys. Res. Lett.*, *46*(15), 8633–8642. https://doi.org/10.1029/2019GL083849

Loto'aniu, T. M., Mann, I. R., Ozeke, L. G., Chan, A. A., Dent, Z. C., and Milling, D. K. (2006). Radial diffusion of relativistic electrons into the radiation belt slot region during the 2003 Halloween geomagnetic storms. *J. Geophys. Res. Space Phys.*, *111*(A4), A04218. https://doi.org/10.1029/2005JA011355

Lyons, L. R., and Williams, D. J. (1984). Quantitative Aspects of Magnetospheric Physics (pp. 79-86). Dordrecht: Springer. https://doi.org/10.1007/978-94-017-2819-5

Mauk, B. H., Fox, N. J., Kanekal, S. G., Kessel, R. L., Sibeck, D. G., and Ukhorskiy, A. (2013). Science objectives and rationale for the Radiation Belt Storm Probes mission. *Space Sci. Rev.*, *179*(1-4), 3–27. https://doi.org/10.1007/s11214-012-9908-y

Mitani, K., Seki, K., Keika, K., Gkioulidou, M., Lanzerotti, L. J., Mitchell, D. G., and Kletzing, C. A. (2018). Radial transport of higher-energy oxygen ions into the deep inner magnetosphere observed by Van Allen Probes. *Geophys. Res. Lett.*, *45*(10), 4534–4541. https://doi.org/10.1029/2018GL077500

Mitchell, D. G., Lanzerotti, L. J., Kim, C. K., Stokes, M., Ho, G., Cooper, S., Ukhorskiy, A., Manweiler, J. W., Jaskulek, S., … Kerem, S. (2013). Radiation belt storm probes ion composition experiment (RBSPICE). *Space Sci. Rev.*, *179*(1-4), 263–308. https://doi.org/10.1007/s11214-013-9965-x

Shi, Q. Q., Hartinger, M., Angelopoulos, V., Zong, Q.-G., Zhou, X. Z., Zhou, X. Y., Kellerman, A., Tian, A. N., Weygand, J., … Yao, Z. H. (2013). THEMIS observations of ULF wave excitation in the nightside plasma sheet during sudden impulse events. *J. Geophys. Res. Space Phys.*, *118*(1), 284–298. https://doi.org/10.1029/2012JA017984

Shi, Q. Q., Hartinger, M. D., Angelopoulos, V., Tian, A. M., Fu, S. Y., Zong, Q.-G., Weygand, J. W., Raeder, J., Pu, Z. Y., … Shen, X. C. (2014). Solar wind pressure pulse-driven magnetospheric vortices and their global consequences. *J. Geophys. Res. Space Phys.*, *119*(6), 4274–4280. https://doi.org/10.1002/2013JA019551

Smith, P. H., and Bewtra, N. K. (1978). Charge exchange lifetimes for ring current ions. *Space Sci. Rev.*, *22*(3), 301–318. https://doi.org/10.1007/BF00239804

Southwood, D. J., Dungey, J. W., and Etherington, R. J. (1969). Bounce resonant interaction between pulsations and trapped particles. *Planet. Space Sci.*, *17*(3), 349–361. https://doi.org/10.1016/0032-0633(69)90068-3

Yang, B., Zong, Q.-G., Fu, S. Y., Li, X., Korth, A., Fu, H. S., Yue, C., and Rème, H. (2011). The role of ULF waves interacting with oxygen ions at the outer ring current during storm times. *J. Geophys. Res. Space Phys.*, *116*(A1), A01203. https://doi.org/10.1029/2010JA015683

Yue, C., Bortnik, J., Li, W., Ma, Q. L., Gkioulidou, M., Reeves, G. D., Wang, C. P., Thorne, R. M., Lui, A. T. Y., … Mitchell, D. G. (2018). The composition of plasma inside geostationary orbit based on Van Allen Probes observations. *J. Geophys. Res. Space Phys.*, *123*(8), 6478–6493. https://doi.org/10.1029/2018JA025344

Yue, C., Bortnik, J., Li, W., Ma, Q. L., Wang, C. P., Thorne, R. M., Lyons, L., Reeves, G. D., Spence, H. E., … Mitchell, D. G. (2019). Oxygen ion dynamics in the earth's ring current: Van Allen probes observations. *J. Geophys. Res. Space Phys.*, *124*(10), 7786–7798. https://doi.org/10.1029/2019JA026801

Zhang, X. Y., Zong, Q.-G., Wang, Y., Zhang, H., Xie, L., Fu, S. Y., Yuan, C. J., Yue, C., Yang, B., Pu, Z. Y. (2010). ULF waves excited by negative/positive solar wind dynamic pressure impulses at geosynchronous orbit. *J. Geophys. Res. Space Phys.*, *115*(A10), A10221. https://doi.org/10.1029/2009JA015016

Zong, Q.-G., Zhou, X. Z., Wang, Y. F., Li, X., Song, P., Baker, D. N., Fritz, T. A., Daly, P. W., Dunlop, M., and Pedersen, A. (2009). Energetic electron response to ULF waves induced by interplanetary shocks in the outer radiation belt. *J. Geophys. Res. Space Phys.*, *114*(A10), A10204. https://doi.org/10.1029/2009JA014393

Zong, Q.-G., Wang, Y. F., Zhang, H., Fu, S. Y., Zhang, H., Wang, C. R., Yuan, C. J., and Vogiatzis, I. (2012). Fast acceleration of inner magnetospheric hydrogen and oxygen ions by shock induced ULF waves. *J. Geophys. Res. Space Phys.*, *117*(A11), A11206. https://doi.org/10.1029/2012JA018024

Zong, Q.-G., Wang, Y. F., Ren, J., Zhou, X. Z., Fu, S. Y., Rankin, R., and Zhang, H. (2017). Corotating drift-bounce resonance of plasmaspheric electron with poloidal ULF waves. *Earth Planet. Phys.*, *1*(1), 2–12. https://doi.org/10.26464/epp2017002